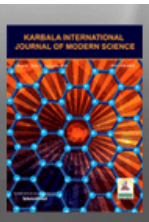

Karbala International Journal of Modern Science

Volume 11 | Issue 3 Article 12

# Synthesis of Cancrinite Zeolite from Toraja Natural Bentonite for Heavy Metal Removal from Wastewater

Yuli Astuti
*1Department of Chemistry, Hasanuddin University, Makassar, Indonesia*

Paulina Taba
*Department of Chemistry, Hasanuddin University, Makassar, Indonesia*, paulinataba@unhas.ac.id

Siti Fauziah
*Department of Chemistry, Hasanuddin University, Makassar, Indonesia*

Syarifuddin Liong
*Department of Chemistry, Hasanuddin University, Makassar, Indonesia,*

Yusafir Hala
*Department of Chemistry, Hasanuddin University, Makassar, Indonesia*

*See next page for additional authors*



## Recommended Citation

Astuti, Yuli; Taba, Paulina; Fauziah, Siti; Liong, Syarifuddin; Hala, Yusafir; Permatasari, Nur Umriani; Negara, Satria Putra Jaya; and Fadliah, Fadliah (2025) "Synthesis of Cancrinite Zeolite from Toraja Natural Bentonite for Heavy Metal Removal from Wastewater," *Karbala International Journal of Modern Science*: Vol. 11 : Iss. 3 , Article 12.
Available at: https://doi.org/10.33640/2405-609X.3420

# Synthesis of Cancrinite Zeolite from Toraja Natural Bentonite for Heavy Metal Removal from Wastewater


## Abstract

This study explores the production of cancrinite (CAN) zeolite from bentonite found in Toraja (a place in South Sulawesi Province, Indonesia) and its effectiveness in removing $Pb^{2+}$ and $Fe^{3+}$ ions from wastewater. The synthesis was carried out using a hydrothermal method with varying NaOH concentrations, where a single phase of zeolite was formed at 5 M, as confirmed through XRD analysis. FTIR results showed the characteristics of CAN zeolite with typical absorption peaks at 676, 622, and 565 $cm^{-1}$, as well as the presence of carbonate groups ($CO_3^{2-}$) at 1300-1400 $cm^{-1}$. SEM analysis revealed thin columnar needle-like crystals characteristic of CAN zeolite. Nitrogen adsorption-desorption tests revealed that CAN zeolite is mesoporous with an average pore size of 5.38 nm and a specific surface area of 51.97 $m^2/g$. The optimal conditions for $Pb^{2+}$ adsorption were achieved with a contact time of 180 minutes and a pH of 5, while for $Fe^{3+}$, the optimal conditions were a contact time of 30 min and a pH of 3. The adsorption isotherm was evaluated using Langmuir, Freundlich, and Sips models, with the best described by the Sips model in non-linear fitting. The maximum adsorption capacities for $Pb^{2+}$ and $Fe^{3+}$ ions were 194.95 mg/g and 196.63 mg/g, respectively. The adsorption kinetics for both ions followed a pseudo-second-order kinetic model. This study reports about natural Toraja bentonite, a rarely explored precursor for CAN zeolite synthesis. It also assesses the zeolite's adsorption capacity for two metal ions of different valences, highlighting its potential in wastewater treatment.



## Keywords

Zeolite, Cancrinite, Adsorption, Heavy metals, Natural bentonite





## Authors

Yuli Astuti, Paulina Taba, Siti Fauziah, Syarifuddin Liong, Yusafir Hala, Nur Umriani Permatasari, Satria Putra Jaya Negara, and Fadliah Fadliah

RESEARCH PAPER

# Synthesis of Cancrinite Zeolite From Toraja Natural Bentonite for Heavy Metal Removal From Wastewater

Yuli Astuti [a], Paulina Taba [a,*], St. Fauziah [a], Syarifuddin Liong [a], Yusafir Hala [a], Nur U. Permatasari [a], Satria P.J. Negara [b], Fadliah [c]

[a] Department of Chemistry, Hasanuddin University, Makassar, Indonesia
[b] Department of Chemistry, State University of Makassar, Makassar, Indonesia
[c] Department of Mining Engineering, Trisakti University, Jakarta, Indonesia

**Abstract**

**This study explores the production of cancrinite (CAN) zeolite from bentonite found in Toraja (a place in South Sulawesi Province, Indonesia) and its effectiveness in removing $Pb^{2+}$ and $Fe^{3+}$ ions from wastewater. The synthesis was carried out using a hydrothermal method with varying NaOH concentrations, where a single phase of zeolite was formed at 5 M, as confirmed through XRD analysis. FTIR results showed the characteristics of CAN zeolite with typical absorption peaks at 676, 622, and 565 $cm^{-1}$, as well as the presence of carbonate groups ($CO_3^{2-}$) at 1300-1400 $cm^{-1}$. SEM analysis revealed thin columnar needle-like crystals characteristic of CAN zeolite. Nitrogen adsorption−desorption tests revealed that CAN zeolite is mesoporous with an average pore size of 5.38 nm and a specific surface area of 51.97 $m^2/g$. The optimal conditions for $Pb^{2+}$ adsorption were achieved with a contact time of 180 min and a pH of 5, while for $Fe^{3+}$, the optimal conditions were a contact time of 30 min and a pH of 3. The adsorption isotherm was evaluated using Langmuir, Freundlich, and Sips models, with the best described by the Sips model in non-linear fitting. The maximum adsorption capacities for $Pb^{2+}$ and $Fe^{3+}$ ions were 194.95 mg/g and 196.63 mg/g, respectively. The adsorption kinetics for both ions followed a pseudo-second-order kinetic model. This study reports about natural Toraja bentonite, a rarely explored precursor for CAN zeolite synthesis. It also assesses the zeolite's adsorption capacity for two metal ions of different valences, highlighting its potential in wastewater treatment.**

*Keywords:* Zeolite, Cancrinite, Adsorption, Heavy metals, Natural bentonite

## 1. Introduction

The concentration of heavy metals in water has risen due to industrial activities, anthropogenic factors, and modern industrialization [1]. Heavy metals are acknowledged to be hazardous and resist natural decomposition, resulting in their accumulation in the environment [2]. Heavy metals in water can negatively impact human health, especially when concentrations exceed permitted limits [3,4]. Heavy metal ions frequently found in industrial effluent include lead ($Pb^{2+}$) and iron ($Fe^{3+}$), usually identified in significant concentrations [5]. $Pb^{2+}$ ions are harmful environmental contaminants that have significant toxic effects on various organs, even at low concentrations [6]. $Fe^{3+}$ ions are essential micronutrients that serve as enzyme cofactors, facilitate oxygen transport, bolster immune system function, and play a role in energy metabolism and cellular growth [7]. The accumulation of $Fe^{3+}$ ions can lead to health issues, including skin and ocular irritation, intestinal wall damage, and respiratory complications. Based on the harm caused by these heavy metal ions, separating and treating of industrial wastewater containing metal ions is necessary to prevent harm to ecological systems and human health.

Various techniques have been used for separation and treatment of wastewater to remove $Pb^{2+}$ and

Received 26 February 2025; revised 21 June 2025; accepted 24 June 2025.
Available online 16 July 2025

* Corresponding author.
E-mail address: Paulinataba@unhas.ac.id (P. Taba).

https://doi.org/10.33640/2405-609X.3420

$Fe^{3+}$ ions, such as membrane separation [8], ion exchange [9,10], chemical precipitation [11], coagulation [12], electrolysis [13], and adsorption [14]. Adsorption is a highly beneficial technique for mitigating metal pollution [15–17]. Adsorption techniques can remove contaminants even at low concentrations, using minimal energy and easily accessible raw materials to create adsorbents from various sources [18,19].

Types of adsorbents that are widely used in wastewater treatment include activated carbon [20], chitosan [21], magnetite [22], mesoporous silica [23], and nanoparticles [24]. However, the limited adsorption capacity and selectivity for certain ions limit their effectiveness. Therefore, zeolites are a promising alternative material for treating wastewater containing heavy metal ions [25].

Zeolites are crystalline, hydrated aluminosilicates with well-defined molecular sieving properties. They are characterized by a high adsorption capacity and large specific surface area. The three-dimensional framework of zeolites is composed of $SiO_4$ and $AlO_4$ tetrahedra linked by shared oxygen atoms, forming cage-like structures and channels [26,27]. The significant adsorption and elevated cation exchange capacity make zeolites particularly effective for removing environmental pollutants [28,29]. The arrangement of zeolite compounds features numerous channels and voids among its molecules, facilitate the diffusion of species into the inter-particle space [30,31]. The application of zeolites as adsorbents has been extensively studied due to their thermal and chemical stability, low environmental friendliness impact, and excellent binding properties. The method for preparing zeolites is straightforward and cost-effective [32].

Zeolites can be obtained naturally or synthesized [33]. Although natural zeolite has been widely used as an adsorbent, its limited availability and variable properties have prompted the development of synthesized zeolite with high purity [34]. Furthermore, the zeolite synthesis process tends to be expensive when using commercial materials, so further research is needed to find alternative, more economical raw materials, such as natural bentonite [32]. As a natural precursor, bentonite can significantly reduce the cost of zeolite synthesis. Its high aluminosilicate content plays a crucial role in minimizing or even eliminating the need for expensive commercial chemical sources, such as sodium silicate and sodium aluminate [35]. Several zeolites synthesized from natural bentonite have been extensively developed and utilized as adsorbents for metal ions. Huang et al. [36] described Na-A zeolite synthesized from bentonite for the adsorption of $Cu^{2+}$ ions, whereas [37] produced ZSM-5 zeolite from bentonite as an adsorbent for $Pb^{2+}$ ions. Moreover [38], successfully synthesized nitrate cancrinite zeolite from natural bentonite. Based on the potential of bentonite as a raw material, these investigations prompted an attempt to synthesize zeolite cancrinite from Toraja bentonite, which has not been extensively researched or utilized as an adsorbent.

Zeolites were synthesized using the hydrothermal technique. The procedure is straightforward and does not require commercial sources of silica-alumina, as reported [39]. The synthesized zeolite was characterized using X-ray fluorescence (XRF), X-ray diffraction (XRD), scanning electron microscopy (SEM), and surface area analyzer (SAA) techniques. A Fourier Transform Infrared (FTIR) spectrophotometer was used to identify functional groups within the zeolite structure. The zeolites produced from this synthesis procedure were then employed as adsorbents for $Pb^{2+}$ and $Fe^{3+}$ ions in the test solution. The effects of contact time, pH, and initial solution concentration were analyzed. The adsorption selectivity of $Pb^{2+}$ and $Fe^{3+}$ ions was examined in a binary solution system. The $Pb^{2+}$ and $Fe^{3+}$ concentrations are quantified in the solution post-adsorption using an Atomic Absorption Spectroscopy (AAS).

## 2. Materials and methods

### 2.1. Materials

The materials used in this study include bentonite, a natural mineral sourced from a mining area in the Toraja district of South Sulawesi, Indonesia (ground to pass through a 200-mesh sieve), NaOH (Merck), $Pb(NO_3)_2$ (Merck), $FeCl_3$ (Merck), $HNO_3$(-Merck), $Na_2EDTA$ (Merck), double distilled water, Whatman 42 filter paper (Merck), and universal pH paper.

### 2.2. Synthesis of CAN zeolites

Zeolite synthesis was conducted under hydrothermal conditions, dissolving 1.4401 g of NaOH in 18 g of water to create a 2 M NaOH solution. Subsequently, 0.7776 g of Toraja natural bentonite (4 % w/w of the mixture) was introduced into the NaOH solution. The mixture was agitated until uniformly distributed, then placed in an autoclave, securely sealed, and exposed to thermal treatment at 170 °C for 24 hrs. After the thermal treatment, the synthesized particles were subjected to vacuum filtration

and rinsed until a neutral pH was reached. The synthesized zeolite underwent a drying process at 105 °C for 24 hrs. Varying concentrations of NaOH, namely 2 M, 3 M, and 5 M, were employed to evaluate their effect on the characteristics of the final product. The synthesized zeolite was then analyzed using XRD, FTIR, SEM, and SAA techniques.

### 2.3. Characterization

The composition of Toraja natural bentonite was analyzed using the XRF method. XRD (Shimadzu XRD-700 with Cu Kα radiation) was used to characterize natural mineral samples and CAN zeolite. FTIR spectra were obtained using a Shimadzu IR Prestige 21, covering the 4000 to 400 $cm^{-1}$ range. The morphology was examined using SEM-EDX (SU-3500). Nitrogen adsorption–desorption isotherms were obtained using a SAA (Altamira micro 200 instrument). The surface area was determined using the Brunauer-Emmett-Teller (BET) method, while the pore size distribution was assessed through the BJH method.

### 2.4. Adsorption experiment

A total of 0.1 g of prepared CAN zeolite was mixed into 50 mL of solution containing $Pb^{2+}$ and $Fe^{3+}$ metal ions. The mixture underwent agitation at 150 rpm for the specified duration. After shaking, the mixture was filtered using filter paper, and the resulting filtrate was analyzed to determine the concentration of metal ions through AAS. Each experiment was conducted in duplicate. The adsorption capacity of the synthesized CAN zeolite for metal ions was evaluated using the following Equation (1):

$$q_e = \frac{C_0 - C_e}{m} V \tag{1}$$

m (g) represents the weight of zeolite CAN, while V (L) denotes the total volume of the metal ion solution.

The main variables influencing the adsorption process were assessed by examining the effects of contact time (3, 5, 10, 20, 30, 60, 90, 120, 180, 210, and 240 mins), pH (1–7), and the initial concentration of the sample solution (25, 50, 100, 150, 200, and 300 mg/L) using a single-variable experimental design. The competitive interaction between $Pb^{2+}$ and $Fe^{3+}$ ions was examined in a binary metal ion system. Each 50 mL metal ion solution was combined and then stirred under the optimal conditions identified for each metal.

### 2.5. Adsorption isotherm

The Langmuir isotherm indicates a monolayer adsorption process at specific active sites on the zeolite surface [40,41]. The Freundlich isotherm describes a multilayer adsorption process on heterogeneous surfaces, characterized by interactions between ions adsorbed on surrounding active sites [42,43]. The Sips isotherm model combines the characteristics of both the Langmuir and Freundlich models and principles of the preceding two models. It is explicitly employed for adsorption systems on heterogeneous surfaces [44,45]. Equations (2)–(6) represent the Langmuir, Freundlich, and Sips linear and non-linear isotherm models, respectively:

$$\frac{C_e}{q_e} = \frac{q_e}{q_m} + \frac{1}{K_L q_m} \tag{2}$$

$$q_e = \frac{q_m K_L C_e}{1 + K_L C_e} \tag{3}$$

The amount of CAN adsorbed is denoted by $q_e$ (mg $g^{-1}$), while $q_m$ (mg $g^{-1}$) represents its adsorption capacity. $K_L$ (L $mg^{-1}$) is the Langmuir adsorption constant, while $C_e$ (mg $L^{-1}$) is the equilibrium concentration of metal ions.

$$q_e = K_f C_e^{\frac{1}{n}} \tag{4}$$

$$\log q_e = \log K_f + \frac{1}{n} \log C_e \tag{5}$$

$K_f$ (mg $g^{-1}$) represents the Freundlich adsorption constant, which is related to adsorption capacity, whereas 1/n indicates the constant that reflects the surface heterogeneity of the adsorbent.

$$q_e = \frac{q_{ms} K_s C_e^{ns}}{1 + K_s C_e^{ns}} \tag{6}$$

$$\ln \frac{q_e}{q_m - q_e} = \ln K_s + \frac{1}{n} \ln C_e \tag{7}$$

$q_m$ (mg $g^{-1}$) represents the maximum adsorption capacity, $K_s$ (L $mg^{-1}$) serves as the Sips equilibrium constant linked to adsorption affinity, and n is the Sips exponent that reflects surface heterogeneity. When n = 1, the surface is homogeneous, making the Sips model equivalent to the Langmuir isotherm.

### 2.6. Adsorption kinetics

Kinetic studies are conducted to assess the dynamics of the adsorption process using rate constants [46]. The adsorption process consists of three

key stages: (i) the movement of the solute from the bulk solution to the boundary layer on the adsorbent surface, (ii) the migration of the solute from the boundary layer onto the adsorbent surface, and (iii) the intraparticle diffusion of the solute from the surface into the internal pore structure of the adsorbent. This investigation examined the adsorption kinetics of $Pb^{2+}$ and $Fe^{3+}$ ions onto synthetic CAN zeolite using linear pseudo-first-order and pseudo-second-order kinetic models. The corresponding mathematical expressions are presented in Equations (8) and (9),

$$\ln(q_e - q_t) = \ln q_e - k_1 t \quad (8)$$

$$\frac{t}{q_t} = \frac{t}{q_e} + \frac{1}{k_2 q^2} \quad (9)$$

k ($min^{-1}$) denotes the adsorption rate constant, t (min) represents the adsorption time, and $q_t$ (mg $g^{-1}$) represents the adsorption capacity at a given time t.

## 3. Result and discussion

### 3.1. Material characterization

Cancrinite zeolite was synthesized using the hydrothermal method with bentonite from Toraja as the raw material. XRF analysis (Table 1) confirmed that the bentonite contains 56.55 % $SiO_2$ and 37.39 % $Al_2O_3$, indicating its suitability for zeolite synthesis due to its high silica and alumina content [32].

The concentration of NaOH significantly influences zeolite synthesis by affecting the skeletal structure. Zeolite synthesis was conducted using Toraja bentonite with NaOH at varying concentrations of 2, 3, and 5 M. Fig. 1a displays data of Toraja bentonite and synthesized zeolite at different NaOH concentrations. Toraja bentonite comprises many minerals, notably quartz, feldspar, and montmorillonite, which serve as its primary constituents. The existence of these compounds is evidenced by the prominent diffraction peaks at angles 2θ = 19.49°, 20.97°, 26.53°, 29.46°, 35.04°, 47.35°, 50.00°, 59.97°, 62.31°, 68.47°, and 74.93° [47].

*Table 1. Chemical composition of Toraja natural bentonite.*

| Wt. % Oxide | $SiO_2$ | $Al_2O_3$ | $K_2O$ | $Fe_2O_3$ | CaO | $TiO_2$ |
|---|---|---|---|---|---|---|
| Natural bentonite | 56.55 | 37.39 | 2.50 | 1.97 | 1.20 | 0.30 |

In the synthesis with a 2 M NaOH concentration, distinct diffraction peaks were observed at 2θ = 15.84°, 20.16°, and 26.01°, indicating the formation of the analcime (ANA) phase [48]. Additional peaks at 2θ = 10.81°, 11.79°, and 30.15° signify the existence of the nepheline hydrate (NHI) phase [49], while peaks at 2θ = 18.86°, 24.24°, and 27.42° validate the formation of the cancrinite (CAN) phase [50]. At 2 M NaOH concentration, three zeolite phases-ANA, NHI, and CAN-were formed. Based on the report by Ref. [51], ANA typically forms at low NaOH concentrations. However, 2 M NaOH is not sufficiently low to produce a pure ANA phase, so the NHI and CAN phases also formed. NHI serve as an intermediate in CAN zeolite synthesis [52]. At 3 M NaOH, the characteristic peak of ANA diminishes, while at 5 M NaOH, only the distinctive peak of CAN remains, confirming that the successful formation of pure CAN zeolite. This result is consistent with [53] report, which states that CAN is more likely to form at high alkali concentrations.

Fig. 1b presents the FTIR spectrum of the Toraja natural bentonite (NB) and zeolite CAN synthesized. The materials exhibit characteristic spectral patterns of aluminosilicates [54]. The synthesized CAN zeolite exhibits a distinct absorption at 3600 $cm^{-1}$. The absorption correlates with hydroxyl groups (O-H) associated with the zeolite structure. A notable absorption shift occurs around 950 $cm^{-1}$, associated with the asymmetric stretching vibrations of the T-O bond, where T denotes Si or Al.

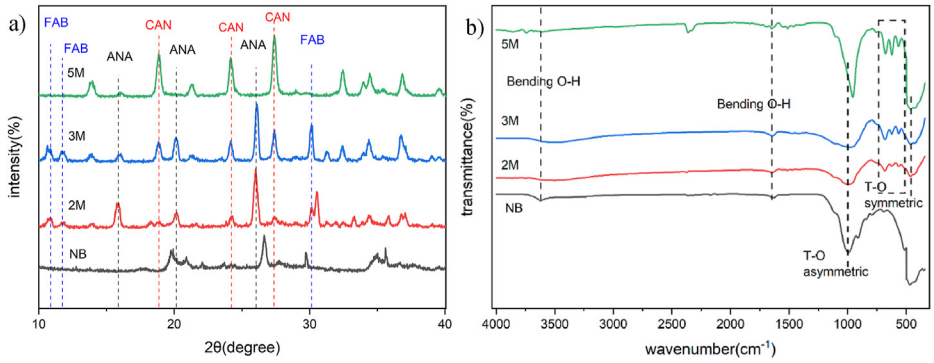


*Fig. 1. a) XRD pattern; and b) FTIR spectra of Toraja natural bentonite and samples synthesized with 2 M, 3 M, and 5 M NaOH.*

The characteristic pattern of zeolite CAN is evident in the absorption peaks observed at 676, 622, and 565 $cm^{-1}$. A weak absorption in the 1300-1400 $cm^{-1}$ range signifies the presence of carbonate groups ($CO_3^{2-}$), characteristic of the structure of CAN zeolites. The presence of $CO_3^{2-}$ groups demonstrates the capacity of CAN zeolites to accommodate large anions within their structure [55,56]. Additionally, the bands observed around 2350 $cm^{-1}$ are attributed to atmospheric $CO_2$, which is detected as a result of the ATR-IR measurement [38].

SEM analysis revealed significant disparities in surface morphology between Toraja bentonite and zeolite synthesized with 5 M NaOH (CAN) following hydrothermal treatment (Fig. 2). Toraja bentonite exhibits a textured structure similar to cornflakes, with a smooth surface, as reported in previous research [57]. The zeolite synthesized with 5 M NaOH exhibited thin columnar crystals resembling needles designated as CAN zeolite [58]. These findings confirm that Toraja bentonite can be converted into CAN zeolite using a hydrothermal method that employs suitable alkaline activators.

Alkaline activators promote the dissolution of silica and alumina oxides from the Toraja bentonite matrix, enabling the production of silica and alumina tetrahedral units that define cancrinite [59].

Based on the EDX analysis (Table 2), there is a significant difference in the Si/Al ratio between natural bentonite and the synthesized CAN zeolite. The Si/Al ratio decreased following synthesis, with the synthesized CAN zeolite exhibiting a Si/Al ratio of 1.27. This result is consistent with previous studies by Refs. [38,60], which reported that the Si/Al ratio of CAN zeolite typically ranges around 1.0.

Type IV adsorption isotherms, indicative of mesoporous materials, were identified in Toraja bentonite and cancrinite [61,62], as illustrated in Fig. 3. The BJH desorption branch patterns substantiate the findings, which affirm that both materials are crystalline mesoporous aluminosilicates with pore sizes ranging from 2 to 50 nm. The synthesis of cancrinite from Toraja bentonite enhanced BET surface area, reaching 51.97 $m^2/g$, alongside a total pore volume of 0.07 cc/g, as detailed in Table 3.

*Table 2. EDX analysis of Toraja natural bentonite and synthesized CAN zeolite (5 M NaOH).*

| Element | Atomic (%) | |
|---|---|---|
| | NB | CAN |
| O | 60.38 | 55.87 |
| Na | 0.02 | 15.29 |
| Mg | 2.77 | – |
| Al | 9.27 | 12.72 |
| Si | 22.11 | 16.13 |
| K | 2.47 | – |
| Ti | 1.12 | – |
| Fe | 1.85 | – |
| Si/Al | 2.39 | 1.27 |

### 3.2. Adsorption of $Pb^{2+}$ and $Fe^{3+}$

Adsorption studies on heavy metals were conducted using $Pb^{2+}$ and $Fe^{3+}$ ions. The adsorption processes were carried out with a contact time of 5–240 mins, a pH range of 1–7, and a concentration of 25–300 mg/L. Fig. 4a shows the effect of contact time on $Pb^{2+}$ and $Fe^{3+}$ ion adsorption using synthetic CAN zeolite. The optimal adsorption time for $Pb^{2+}$ and $Fe^{3+}$ ions was achieved at 30 mins and 180 mins, respectively. This optimal time indicates that the adsorption of $Fe^{3+}$ ions occurs more rapidly with synthesized CAN zeolite than $Pb^{2+}$ ions. This difference is attributed to the higher positive charge of $Fe^{3+}$, which enhances electrostatic interactions with negatively charged active sites on the zeolite surface, thereby facilitating faster adsorption [63,64]. After this period, adsorption capacity decreased, signifying the saturation of active sites on the CAN zeolite and the weakening of electrostatic

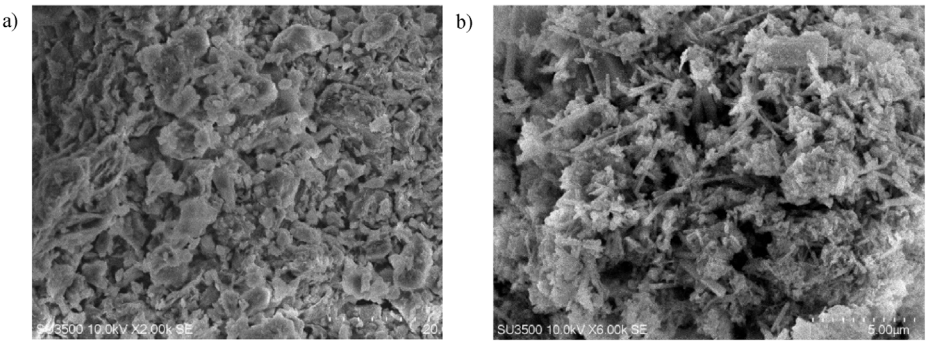


*Fig. 2. SEM image of a) Toraja natural bentonite b) synthesized CAN zeolite (5 M NaOH).*

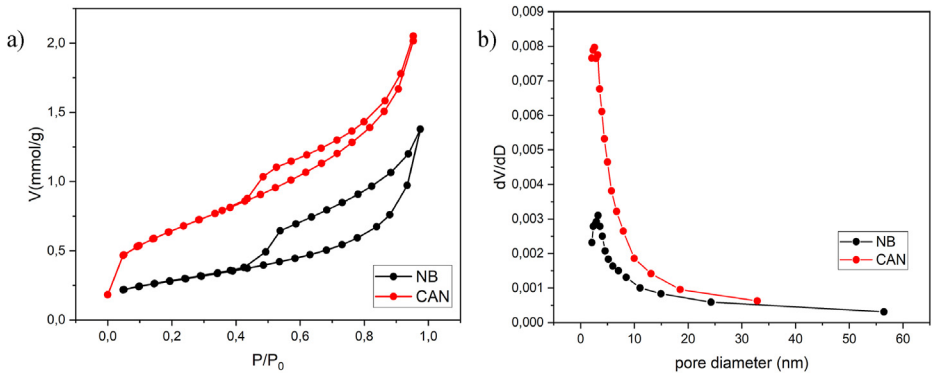


*Fig. 3. a) The $N_2$ isotherm adsorption–desorption characteristics; b) pore size distribution analysis of Toraja natural bentonite and synthesized CAN zeolite.*

*Table 3. Surface area and porosity of Toraja natural bentonite and synthesized CAN zeolite (5M NaOH).*

| Materials | BET surface area ($m^2$/g) | Total pore volume | Average pore size (nm) |
|---|---|---|---|
| NB | 22.05 | 0.05 | 8.67 |
| CAN | 51.97 | 0.07 | 5.38 |

interactions between $Pb^{2+}$ and $Fe^{3+}$ ions and the zeolite surface.

The adsorption of metal ions in solution is significantly impacted by pH because metal cations and $H^+$ ions compete for active sites on the adsorbent surface [65]. The adsorption of $Fe^{3+}$ ions reached its optimal pH at 3, while $Pb^{2+}$ ions achieved theirs at 5 (Fig. 4b). The removal effectiveness of $Fe^{3+}$ ions is greater under acidic conditions than $Pb^{2+}$, which is related to the higher charge on $Fe^{3+}$, making it more prone to hydration in aqueous environments and more stable at low pH. Both $Fe^{3+}$ and $Pb^{2+}$ ions exhibit similar adsorption behaviors, with maximum effectiveness occurring at a pH that is neither excessively acidic nor basic. Under very acidic conditions, competition between $H^+$ ions and metal cations reduce metal ion binding on the

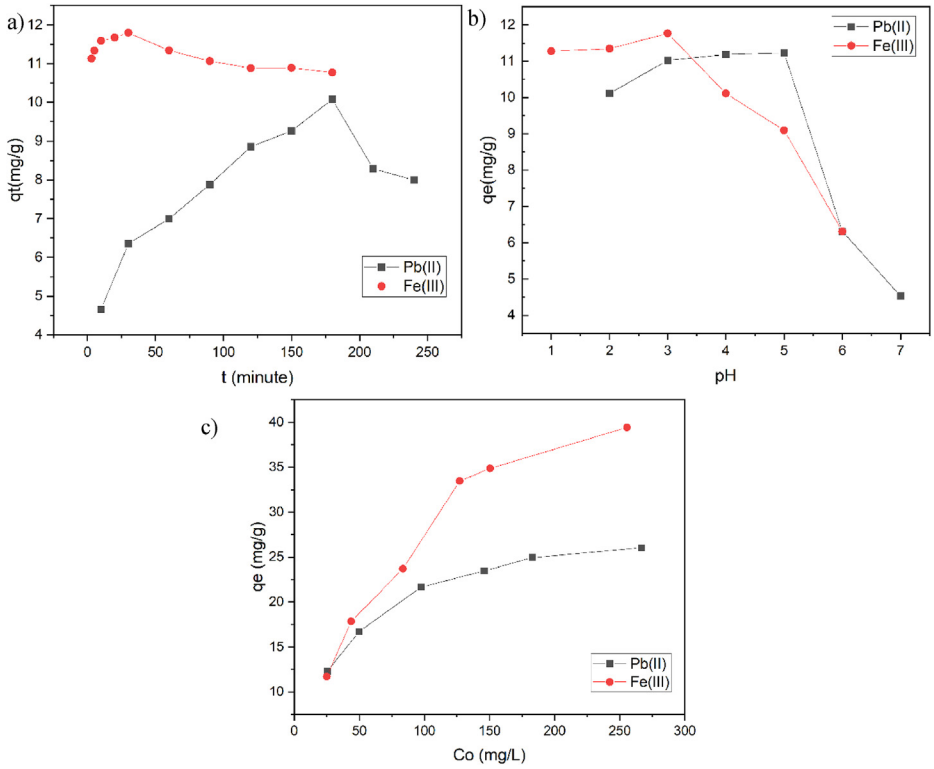


*Fig. 4. Graph illustrating the correlation between a) adsorption time; b) pH of solution; c) concentration and the total of adsorbed $Pb^{2+}$ and $Fe^{3+}$ ions by synthesized CAN zeolite.*

adsorbent. Excess $H^+$ ions may interact with the active sites of the material, obstructing metal ion adsorption. Conversely, at near-neutral pH, increased $OH^-$ ion concentration can lead to metal ion precipitation as hydroxides, reducing adsorption efficiency [66].

Adsorption analysis reveals that increasing metal ion concentration enhances adsorption capacity [67]. The elevated concentration facilitates the migration of metal ions from the solution into the zeolite pores. The adsorption process is influenced by the absorbency and pore structure of zeolite. Metal ions penetrate the zeolite pores via interactions with the $[SiO_4]^{4-}$ and $[AlO_4]^{5-}$ structures within the zeolite framework. Metal ions confined within the pores and adhered to the zeolite contribute to the solution's decreased metal ion concentration. Fig. 4c shows that CAN synthetic zeolite adsorbs $Fe^{3+}$ more effectively than $Pb^{2+}$. This difference is influenced by the physicochemical properties of the metal ions, as well as the surface characteristics and pore structure of the zeolite. In this study, the large pore size of the zeolite enables metal ions to penetrate the pore system and interact with active sites. $Fe^{3+}$ ions have a greater hydration diameter and hydration energy than $Pb^{2+}$; however, the higher adsorption capacity of the zeolite for $Fe^{3+}$ ions can be attributed to the higher ionic charge, which generates a strong electrostatic attractive force toward negatively charged active sites. Additionally, the sizable pore size of the zeolite and its surface chemical affinity for $Fe^{3+}$ further enhance adsorption efficiency [68].

The adsorption of heavy metals onto zeolites occurs through several processes, including ion exchange, diffusion, and interactions with hydroxyl groups [66,69]. Ion exchange transpires between heavy metal ions and the exchangeable cations within the zeolite framework. For instance, $Na^+$ ions participate in the following reaction:

$$R\text{-}Na + X \leftrightarrow R\text{-}X + Na^+$$

Besides ion exchange, the adsorption mechanism involves interfacial interactions occurring on the zeolite surface. Interactions occur between hydroxyl groups and heavy metal ions, including hydrogen bonding and van der Waals forces. These interactions influence the stability of metal ions on the adsorbent surface. Moreover, diffusion mechanisms significantly contribute to the adsorption process, particularly with $Pb^{2+}$ and $Fe^{3+}$ ions. Metal ions traverse the channels and cavities of zeolite micropores according to the principle of selective screening, referred to as molecular sieving events [69].

### 3.3. Adsorption isotherm

Fig. 5 illustrates the linear adsorption isotherm curves derived from the Langmuir, Freundlich, and Sips models for the adsorption of $Pb^{2+}$ and $Fe^{3+}$ ions by the synthesized CAN zeolite. Table 4 presents the derived linear isotherm parameters. The study shows that the Langmuir isotherm model offers the best fit for the adsorption of $Pb^{2+}$ and $Fe^{3+}$ ions by synthesized CAN zeolite, with $R^2$ values closest to 1.

The Langmuir adsorption model outlines the process of a single saturated layer of solute molecules adhering to the adsorbent surface while disregarding any lateral interactions between adsorbed molecules. Adsorption occurs on a structurally homogenous adsorbent, forming a monolayer on the particle surface [41,70]. The separation factor ($R_L$) for metal ion adsorption by synthesized CAN zeolite, derived from Fig. 5a, ranged from 0.02 to 0.1, indicating values less than 1. The $R_L$ values suggest that the Langmuir model accurately characterizes the adsorption [71] of $Pb^{2+}$ and $Fe^{3+}$ ions by the synthesized CAN zeolite. The maximum adsorption capacity for both metal ions was determined using the Langmuir equation. The adsorption capacity for $Pb^{2+}$ was 26.52 mg/g, whereas $Fe^{3+}$ had an adsorption capacity of 42.02 mg/g, exceeding that of $Pb^{2+}$. The ionic radii of $Pb^{2+}$ and $Fe^{3+}$ are 0.119 nm and 0.065 nm, respectively.

The difference in radius affects the hydration diameter of the ions, where $Pb^{2+}$ ions have a smaller hydration diameter than $Fe^{3+}$ ions. In theory, ions with smaller hydration diameters are more easily adsorbed because they experience lower diffusion resistance. However, the results of this study did not fully follow this trend. Zeolite CAN exhibits a higher adsorption capacity for $Fe^{3+}$ than for $Pb^{2+}$. These findings align with previous studies suggesting that ions with larger radii and higher molecular masses, such as $Pb^{2+}$, may saturate adsorbent pores or active sites more rapidly, thereby reducing adsorption capacity [70,72].

Fig. 5b and Table 4 illustrate the adsorption effects of $Pb^{2+}$ and $Fe^{3+}$ ions using the synthesized CAN zeolite, integrating with the Freundlich isotherm model. The Freundlich isotherm describes the adsorption process on heterogeneous surfaces [43,73]. The heterogeneity factor ($n = 1/n_f$) correlates with the adsorption intensity, which depends on the material's heterogeneity. According to Fig. 5b and Table 4, the value of $1/n_f$ for both ions is less than 1.

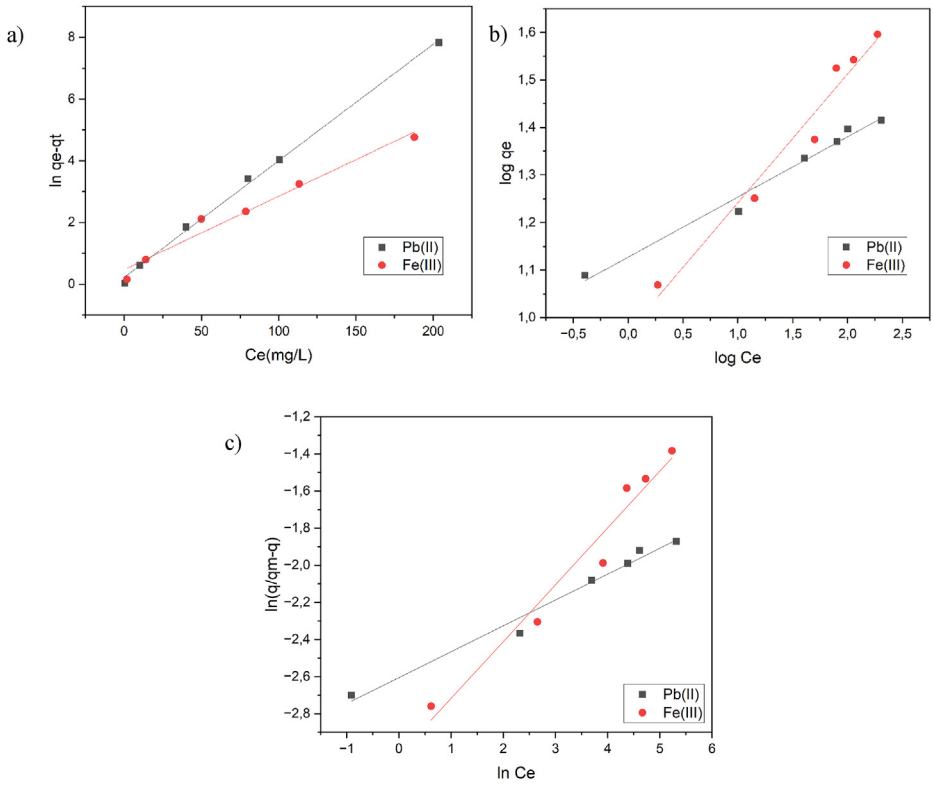


*Fig. 5. Linear adsorption isotherms of a) Langmuir, b) Freundlich, and c) Sips for the adsorption of $Pb^{2+}$ and $Fe^{3+}$ metal ions by synthesized CAN zeolite.*

*Table 4. Specifications of the linear adsorption isotherm for $Pb^{2+}$ and $Fe^{3+}$ ions adsorbed by synthesized CAN zeolite.*

| Model | Parameters | Metal ions | |
|---|---|---|---|
| | | $Pb^{2+}$ | $Fe^{3+}$ |
| Langmuir | $K_L$ | 0.1712 | 0.0503 |
| | $q_m$ | 26.5252 | 42.0168 |
| | $R^2$ | 0.9978 | 0.9734 |
| Freundlich | $K_f$ | 13.4153 | 9.3584 |
| | $n_f$ | 7.9177 | 3.6928 |
| | $R^2$ | 0.9821 | 0.9674 |
| Sips | $K_s$ | 0.0965 | 0.0366 |
| | $n_s$ | 1,1787 | 3.2669 |
| | $q_m$ | 194.9483 | 196.626 |
| | $R^2$ | 0.9803 | 0.9615 |

The $1/n_f$ values suggest that $Pb^{2+}$ and $Fe^{3+}$ adsorption on synthesized CAN zeolite conforms to the Freundlich isotherm model, indicating favorable adsorption [74].

The Sips isotherm model (Fig. 5c) integrates the Langmuir and Freundlich equations to enhance understanding of the behavior of homogeneous and heterogeneous adsorption systems [75]. Furthermore, the Sips model addresses the shortcomings of the Freundlich isotherm model at elevated adsorbate concentrations. The Sips model resembles the Freundlich isotherm at low adsorbate concentrations. Nevertheless, the Langmuir isotherm [42] suggests that single-layer adsorption is likely when a substantial amount of adsorbate is present. The $q_{max}$ values for $Pb^{2+}$ and $Fe^{3+}$ ions derived from the Sips model exceeded those obtained from the Langmuir model (refer to Table 4).

The adsorption isotherms were modeled using nonlinear equations for the Langmuir, Freundlich, and Sips models to improve result accuracy. Fig. 6a and b illustrate the three adsorption models for $Pb^{2+}$ and $Fe^{3+}$ ions on synthesized CAN zeolite, with adsorption details provided in Table 5. Modelling adsorption isotherms with non-linear equations primarily evaluates the Sum of Squared Residuals (SSR). SSR measures the model's accuracy in comparison to the experimental data. A lower SSR value signifies enhanced consistency between the model and the empirical data.

The examination of SSR values (see Table 5) suggests that the Sips isotherm model best describes the adsorption of $Pb^{2+}$ and $Fe^{3+}$ ions by synthesized CAN zeolite, as it presents the lowest SSR value relative to the Langmuir and Freundlich models. The Sips isotherm model quantifies heterogeneity in the adsorption system. This heterogeneity can arise from the properties of the solid (adsorbent), the adsorbate, or a combination of both, as shown by the

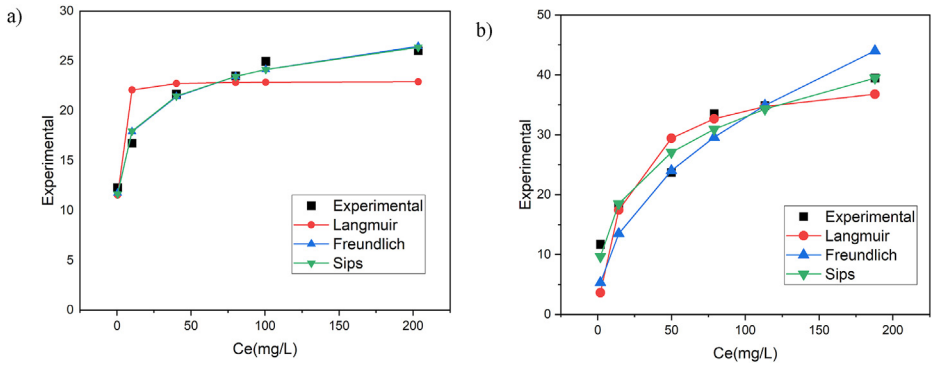


*Fig. 6. Non-linear adsorption isotherms of Langmuir, Freundlich, and Sips for the adsorption of, a) $Pb^{2+}$ and b) $Fe^{3+}$ metal ions by synthesized CAN zeolite.*

*Table 5. Specifications of the non-linear adsorption isotherm for $Pb^{2+}$ and $Fe^{3+}$ ions adsorbed by synthesized CAN zeolite.*

| Model | Parameter | Metal ions | |
|---|---|---|---|
| | | $Pb^{2+}$ | $Fe^{3+}$ |
| Langmuir | $K_L$ | 2.5138 | 0.0533 |
| | $q_m$ | 22.9545 | 40.4532 |
| | $R_L$ | 0.0056 | 0.1858 |
| | $R^2$ | 0.9993 | 0.9734 |
| | SSR | 44,6591 | 105.9124 |
| Freundlich | $K_f$ | 13.2424 | 4.0098 |
| | $n_f$ | 7.6810 | 2.1855 |
| | $R^2$ | 0.9971 | 0.9830 |
| | SSR | 2.5228 | 96.0983 |
| Sips | $K_s$ | 0.0725 | $9.39 \times 10^{-5}$ |
| | $n_s$ | 0.1449 | 0.3422 |
| | $q_m$ | 194.9483 | 196.626 |
| | $R^2$ | 0.9949 | 0.9914 |
| | SSR | 2.1990 | 22.9527 |

heterogeneity exponent $n_s$. If $n_s$ is close to 1, it suggests that the solid has relatively homogeneous adsorption sites. If $n_s < 1$, the system exhibits greater heterogeneity and corresponds more closely with the Freundlich isotherm model. The $n_s$ values for $Pb^{2+}$ and $Fe^{3+}$ ions indicate that the adsorption system aligns more closely with the Freundlich isotherm model, reflecting the characteristics of a heterogeneous adsorbent surface. Modeling results revealed that the Sips isotherm model has a maximum adsorption capacity of 194.9 mg/g for $Pb^{2+}$ and 196.6 mg/g for $Fe^{3+}$. The comparison of maximum adsorbed amount of $Pb^{2+}$ and $Fe^{3+}$ ions on examined materials surface with others zeolites and natural minerals is presented in Table 6.

### 3.4. Adsorption kinetics

Fig. 7 illustrates the experimental and predicted outcomes using linear first-order and second-order pseudo-kinetic models for the adsorption of $Pb^{2+}$ and $Fe^{3+}$ ions by synthesized CAN zeolite. The parameters of these kinetic models are outlined in

*Table 6. Comparison of adsorption capacity of metal ions on the examined solids surface with others zeolite and natural mineral.*

| Adsorbent | Adsorbate | Adsorption capacity | References |
|---|---|---|---|
| CAN zeolite from Kaolinite | $Pb^{2+}$ | 192 | [76] |
| K-type zeolite from Fly ash | $Pb^{2+}$ | 55.53 | [77] |
| Azide CAN from zeolite K | $Pb^{2+}$ | 52.63 | [78] |
| Zeolite A from waste LD-slag | $Fe^{3+}$ | 27.55 | [79] |
| Zeolite 4A waste | $Fe^{3+}$ | 95.18 | [80] |
| Natural zeolite | $Fe^{3+}$ | 1.18 | [81] |
| Brown bentonite | $Fe^{3+}$ | 16.65 | [82] |
| Natural bentonite from Slovakia | $Pb^{2+}$ | 32.68 | [83] |
| Na-type zeolite from Coal Gastification slag | $Pb^{2+}$ | 10.00 | [66] |
| CAN zeolite from Toraja Bentonite | $Pb^{2+}$ | 194.95 | This study |
| CAN zeolite from Toraja Bentonite | $Fe^{3+}$ | 196.63 | This study |

Table 7. The pseudo-second-order kinetic model demonstrated a better fit in describing the adsorption of $Pb^{2+}$ and $Fe^{3+}$ ions, as indicated by higher $R^2$ values compared to the pseudo-first-order kinetic model. Moreover, the $q_e$ values predicted by this model closely aligned with the $q_e$ values derived from experimental observations, confirming that the pseudo-second-order model was the best fit [66,84]. These findings confirm that the removal of $Pb^{2+}$ and $Fe^{3+}$ ions using synthesized CAN zeolite occurs through a chemisorption mechanism. This mechanism results from a combination of electrostatic forces and chemical interactions, including covalent bonding, ion exchange, and complexation between the metal ions and the zeolite surface.

### 3.5. Adsorption selectivity

The adsorption selectivity was assessed to determine the capacity of synthesized CAN zeolite to

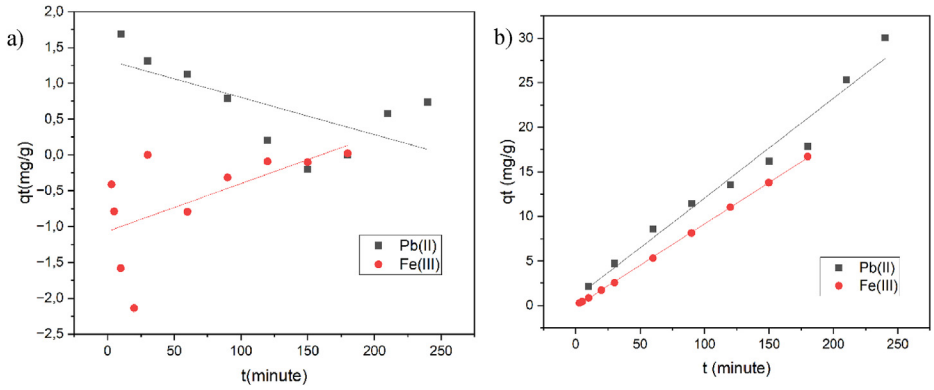


*Fig. 7. Kinetics of $Pb^{2+}$ and $Fe^{3+}$ metal ion adsorption by synthesized CAN zeolite. a) pseudo-first-order; b) pseudo-second-order.*

*Table 7. Specifications of the adsorption kinetics for $Pb^{2+}$ and $Fe^{3+}$ ions adsorbed by synthesized CAN zeolite.*

| Metal ions | Pseudo-first order | | | Pseudo-second order | | |
|---|---|---|---|---|---|---|
| | $K_1$ | $q_e$ | $R^2$ | $K_2$ | $q_e$ | $R^2$ |
| $Pb^{2+}$ | 0.0052 | 3.7449 | 0.4452 | 0.0110 | 8.9445 | 0.9694 |
| $Fe^{3+}$ | 0.0067 | 0.3445 | 0.3522 | 0.0010 | 10.7757 | 0.9997 |

adsorb $Pb^{2+}$ and $Fe^{3+}$ ions in both single-ion and binary systems. In the binary system, solutions containing $Pb^{2+}$ and $Fe^{3+}$ ion concentrations of 25 mg/L each in 50 mL of solution were prepared and processed under the optimal conditions for each metal ion.

Fig. 8a illustrates the adsorption selectivity of $Pb^{2+}$ and $Fe^{3+}$ ions in a single system, presented as the relationship between pH and adsorption capacity. The optimum pH of each ion indicates that pH influences the adsorption selectivity [85] of $Pb^{2+}$ and $Fe^{3+}$ ions. $Fe^{3+}$ ions exhibit greater selectivity at acidic pH compared to $Pb^{2+}$ ions due to $Fe^{3+}$'s elevated hydration potential, which facilitates the formation of aqua complexes in the presence of sufficient $H^+$ ions [86]. This condition also inhibits the hydrolysis of $Fe^{3+}$ ions, which typically hydrolyze at pH levels around neutrality, allowing $Fe^{3+}$ to interact effectively with zeolite active sites [87].

Conversely, $Pb^{2+}$ ions exhibits greater stability in its ionic form near neutral pH, making it more accessible for adsorption by zeolites. The interaction between zeolite and metal with metal ions is more favorable at near-neutral pH than at acidic pH, when the protonation of zeolite's active groups occurs [88,89]. In addition, the hydration diameter of metal ions significantly influences the adsorption selectivity of $Pb^{2+}$ and $Fe^{3+}$ ions by CAN zeolites [90]. Compared to the zeolite pore size (5.38 nm), the hydration diameter of $Pb^{2+}$ ions is approximately 0.40 nm, while that $Fe^{3+}$ ions is roughly 0.90 nm. Heavy metal ions can readily penetrate the zeolite pore and interact with the cations within, depending on zeolite pore size and the metal hydration radius.

Adsorption selectivity is also affected by the electronegativity of the metal [91]. $Pb^{2+}$ ions exhibit a higher electronegativity (2.33) than $Fe^{3+}$ (1.83), which presumably enhances their interaction with the active sites of the adsorbent. A higher electronegativity of an ion correlates with stronger interaction with the zeolite surface [92].

Although $Pb^{2+}$ has a smaller hydration diameter and higher electronegativity than $Fe^{3+}$ ions, experimental results show that $Fe^{3+}$ is more selectively adsorbed than $Pb^{2+}$ in the single system (see Fig. 8a). $Fe^{3+}$ is more selective than $Pb^{2+}$, which may

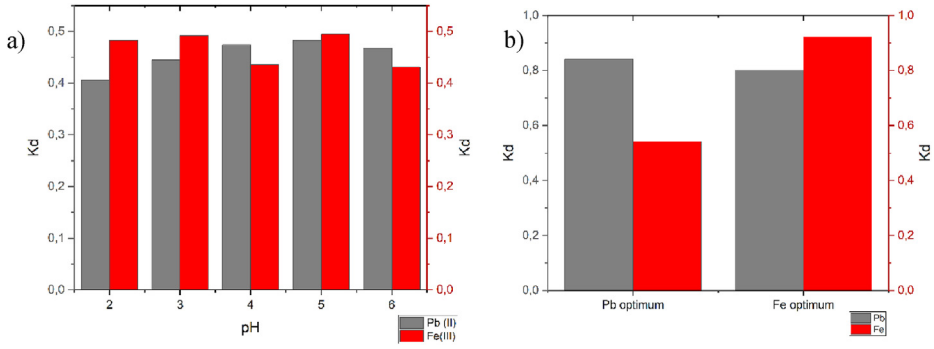


*Fig. 8. Adsorption selectivity of metal ions in (a) single metal systems; (b) binary systems.*

be due to the size mismatch between $Pb^{2+}$ hydration and zeolite pores, allowing ions with larger diameters to be more easily adsorbed [68]. In addition, the larger charge of $Fe^{3+}$ ions lead to stronger electrostatic interactions with the zeolite active groups, increasing the adsorption efficiency.

The difference in adsorption selectivity in the binary system is shown in Fig. 8b. In the $Fe^{3+}$-$Pb^{2+}$ system, $Fe^{3+}$ acts as the target ion, while $Pb^{2+}$ is the competitor ion. The adsorption selectivity of $Pb^{2+}$ is 0.80, and $Fe^{3+}$ is 0.92, showing a high value at $Fe^{3+}$'s optimum condition. CAN zeolite more effectively adsorb $Pb^{2+}$ due to its lower hydration energy and higher electronegativity than $Fe^{3+}$ [93]. In contrast, in the $Pb^{2+}$-$Fe^{3+}$ system, $Pb^{2+}$ acts as the target ion, while $Fe^{3+}$ is the competitor ion. The adsorption selectivity of $Fe^{3+}$ (0.54) is lower than that of $Pb^{2+}$ (0.84), indicating that $Fe^{3+}$ is less competitive with $Pb^{2+}$. CAN zeolite only adsorbs $Fe^{3+}$ if the $Pb^{2+}$ concentration is insufficient to achieve adsorption saturation. Based on the selectivity of the binary system, it can be concluded that $Pb^{2+}$ has a higher adsorption selectivity than $Fe^{3+}$ in the presence of competitor ions.

### 3.6. Desorption and regeneration

The reuse of adsorbents is an essential factor in assessing their potential applications. This study conducted adsorption–desorption experiments to evaluate recovery efficiency and assess the reusability of the synthesized zeolite. The desorption performance of the synthesized CAN zeolite was evaluated using 0.1 M $HNO_3$, 0.1 M $Na_2EDTA$, and $H_2O$ solutions. The desorption behavior of $Pb^{2+}$ and $Fe^{3+}$ ions from the synthesized CAN zeolite is illustrated in Fig. 9a.

According to the desorption data in Fig. 9a, the 0.1 M $HNO_3$ solution demonstrated the highest efficacy in desorbing $Pb^{2+}$ and $Fe^{3+}$ ions, achieving 85.09 % and 77.18 %, respectively. The acidic condition causes protonation of the adsorbent surface, further facilitating the release of positively charged metal ions [94]. Sari et al. [95] indicated that $HNO_3$ serves as an effective desorption agent due to the high-affinity $NO_3^-$ ions, which promote the formation of stable complexes with $Pb^{2+}$ and $Fe^{3+}$ ions. During adsorption, cations on the CAN zeolite are substituted by $Pb^{2+}$ and $Fe^{3+}$ ions. Conversely, in the desorption phase, $Pb^{2+}$ and $Fe^{3+}$ ions are released from zeolite surface and re-enter the solution.

$Na_2EDTA$ desorption agent effectively releases $Pb^{2+}$ and $Fe^{3+}$ ions, achieving 77.20 % and 66.37 % desorption, respectively. The desorption process occurs as ligands in the $Na_2EDTA$ solution donate electrons through two oxygen and four nitrogen atoms, forming a stable six-ringed chelate complex. The process makes $Na_2EDTA$ an effective desorption agent for metal ions [96,97]. In contrast, desorption using $H_2O$ shows a lower percentage because it cannot participate in competitive ion exchange. As a neutral solvent, $H_2O$ does not provide sufficient $H^+$ ions to protonate the adsorbent surface, causing metal ions to remain bound to the zeolite. These results align with research conducted by Ref. [98], which reported that desorption of metal ions is more effective in acidic conditions compared to neutral conditions.

The reuse study of CAN zeolite was conducted twice using $HNO_3$, identified as the most suitable desorption agent from the previous experiment, as illustrated in Fig. 9b. The adsorption efficiency of $Pb^{2+}$ and $Fe^{3+}$ metal ions by CAN zeolite decreased significantly from the first to the second cycle, by approximately 25 %. After two regeneration cycles, efficiency declined considerably, possibly due to structural damage caused by exposure to acidic media [99]. These results are in line with research conducted [100], which examined the regeneration of $Pb^{2+}$ metal ions on zeolites from coal fly ash using $HNO_3$ solution. The study reported a decreased in adsorbent mass, indicating physical changes and structural damage due to acid exposure.

In addition, the lower desorption efficiency compared to the adsorption efficiency in the

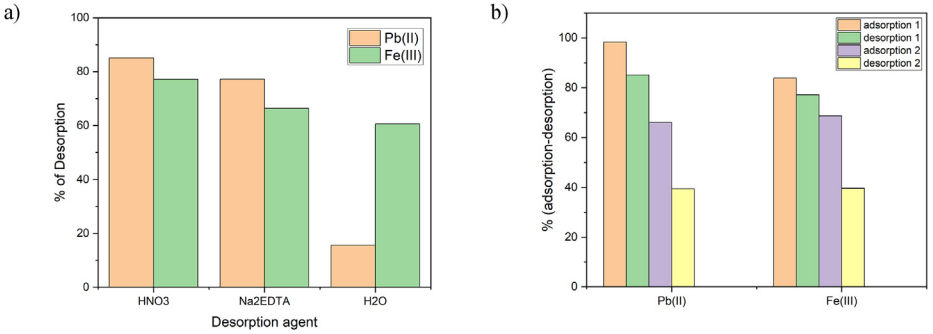


*Fig. 9. (a) Desorption of $Pb^{2+}$ dan $Fe^{3+}$ ion using desorption agent; (b) Reuse cycle of zeolite CAN on $Pb^{2+}$ and $Fe^{3+}$ adsorption–desorption.*

adsorption–desorption cycle indicates heterogeneity on the zeolite surface [101,102]. Some active sites on zeolites exhibit higher binding energy, allowing ions to form strong bonds that are difficult to desorb [103]. These findings suggest that the synthesized CAN zeolite still requires further modification to improve its reusability. A similar study [104] also tested the regeneration of CFAZ magnetite composites for $Pb^{2+}$ metal ions over 3–4 regeneration cycles.

## 4. Conclusion

Cancrinite zeolite was effectively synthesized from Toraja natural bentonite via hydrothermal process with the incorporation of sodium hydroxide. This zeolite has proven effective as an adsorbent for removing $Pb^{2+}$ and $Fe^{3+}$ ions from wastewater. The optimization of process parameters, such as contact time, pH level, and initial concentration of metal ions, enhanced adsorption capacity until equilibrium was attained. Adsorption adhered to the Sips isotherm model, whereas the kinetics of adsorption conformed to a pseudo-second-order model. Selective experiments indicated that the zeolite exhibited more excellent selectivity for $Fe^{3+}$ compared to $Pb^{2+}$ in a single system but was more selective for $Pb^{2+}$ than $Fe^{3+}$ in a binary system. Consequently, CAN zeolite exhibits potential as an effective adsorbent for treating wastewater containing $Pb^{2+}$ and $Fe^{3+}$ ions. For future research, it is recommended to conduct a detailed investigation the mechanism of metal ion adsorption by zeolites, particularly in relation to pH conditions, as this factor has a significant impact on adsorption. To assess the adsorbent ability of CAN zeolite in alignment with eco-friendly and cost-effective principles, it is crucial to further examine the regeneration and reutilization of synthetic zeolite. Additionally, the production of composites with synthetic zeolites may present an opportunity to enhance adsorption ability.

## Ethics information

This study involved no human or animal subjects. All experiments focused on synthesizing and characterizing zeolites from natural minerals and evaluating their adsorption of Pb(II) and Fe(III) ions in aqueous solutions. All procedures complied with institutional safety and environmental standards.

## Funding

This research was supported by Hasanuddin University grant for the 2024 fiscal on contract agreement number: 00309/UN4.22/PT.01.03/2024 dated January 30, 2024.

## Conflicts of interest

The authors assert that they possess no recognized competing financial interests or personal relationships that may have seemingly influenced the work presented in this study.

## Acknowledgements

The author is grateful to Hasanuddin University grant for the 2024 fiscal based on contract agreement number: 00309/UN4.22/PT.01.03/2024 dated January 30, 2024.

## References

[1] K.H.H. Aziz, F.S. Mustafa, K.M. Omer, S. Hama, R.F. Hamarawf, K.O. Rahman, Heavy metal pollution in the aquatic environment: efficient and low-cost removal approaches to eliminate their toxicity: a review, RSC Adv 13 (26) (2023) 17595–17610, https://doi.org/10.1039/D3RA00723E.

[2] H. Ali, E. Khan, I. Ilahi, Environmental chemistry and ecotoxicology of hazardous heavy metals: environmental persistence, toxicity, and bioaccumulation, J. Chem. (1) (2019) 1–14, https://doi.org/10.1155/2019/6730305.

[3] B. Nedjimi, Phytoremediation: a sustainable environmental technology for heavy metals decontamination, SN Appl. Sci. 3 (3) (2021) 1–19, https://doi.org/10.1007/s42452-021-04301-4.

[4] S. Mitra, A.J. Chakraborty, A.M. Tareq, T. Bin Emran, F. Nainu, A. Khusro, A.M. Idris, M.U. Khandaker, H. Osman, F.A. Alhumaydhi, J. Simal-Gandara, Impact of heavy metals on the environment and human health: novel therapeutic insights to counter the toxicity, J. King Saud Univ. Sci. 34 (3) (2022) 1–23, https://doi.org/10.1016/j.jksus.2022.101865.

[5] E. Matei, A.M. Predescu, A.A. Şăulean, M. Râpă, M.G. Sohaciu, G. Coman, A.-C. Berbecaru, C. Predescu, D. Vâju, G. Vlad, Ferrous industrial wastes—valuable resources for water and wastewater decontamination, Int. J. Environ. Res. Public Health. 19 (21) (2022) 1–25, https://doi.org/10.3390/ijerph192113951.

[6] V. Shukla, P. Shukla, A. Tiwari, Lead poisoning, Indian J. Med. Spec. 9 (3) (2018) 146–149, https://doi.org/10.1016/j.injms.2018.04.003.

[7] E. Piskin, D. Cianciosi, S. Gulec, M. Tomas, E. Capanoglu, Iron absorption: factors, limitations, and improvement methods, ACS Omega 7 (24) (2022) 20441–20456, https://doi.org/10.1021/acsomega.2c01833.

[8] A.H. Birniwa, S. Habibu, S.S. Abdullahi, R.E.A. Mohammad, A. Hussaini, H. Magaji, B.N.S. Al-dhawi, A. Noor, A.H. Jagaba, Membrane technologies for heavy metals removal from water and wastewater: a mini review, Case Stud. Chem. Environ. Eng. 9 (2024) 1–15, https://doi.org/10.1016/j.cscee.2023.100538.

[9] A. Bashir, L.A. Malik, S. Ahad, T. Manzoor, M.A. Bhat, G.N. Dar, A.H. Pandith, Removal of heavy metal ions from aqueous system by ion-exchange and biosorption methods, Environ. Chem. Lett. 17 (2) (2019) 729–754, https://doi.org/10.1007/s10311-018-00828-y.

[10] M.S. Chauhan, A.K. Rahul, S. Shekhar, S. Kumar, Removal of heavy metal from wastewater using ion exchange with membrane filtration from Swarnamukhi river in Tirupati, Mater. Today Proc. 78 (2023) 1–6, https://doi.org/10.1016/j.matpr.2022.08.280.

[11] A. Pohl, Removal of heavy metal ions from water and wastewaters by sulfur-containing precipitation agents, Water, Air, Soil Pollut. 231 (10) (2020) 1–17, https://doi.org/10.1007/s11270-020-04863-w.

[12] M.Y.D. Alazaiza, A. Albahnasawi, O. Almaskari, T. Almaskari, M.S.S. Abujazar, S.S. Abuamr, D.E. Nassani, Role of natural coagulants in the removal of heavy metals from different wastewaters: principal mechanisms, applications, challenges, and prospects, Glob. NEST J. 24 (4) (2022) 594–606, https://doi.org/10.30955/gnj.004478.
[13] N. Gomelya, Y. Melnychenko, I. Radovenchyk, Purification of wastewater from the ions of copper, zinc, and lead using an electrolysis method, Eastern-European J. Enterp, Technol. 6 (10) (2018) 42–48, https://doi.org/10.15587/1729-4061.2018.148896.
[14] A.M.P. Madhubashani, D.A. Giannakoudakis, B.M.W.P.K. Amarasinghe, A.U. Rajapaksha, P.B.T. Pradeep Kumara, K.S. Triantafyllidis, M. Vithanage, Propensity and appraisal of biochar performance in removal of oil spills: a comprehensive review, Environ. Pollut. 288 (2021) 1–22, https://doi.org/10.1016/j.envpol.2021.117676.
[15] A.K. Thakur, R. Singh, R. Teja Pullela, V. Pundir, Green adsorbents for the removal of heavy metals from Wastewater: a review, Mater, Today Proc. 57 (2022) 1468–1472, https://doi.org/10.1016/j.matpr.2021.11.373.
[16] N.A.A. Qasem, R.H. Mohammed, D.U. Lawal, Removal of heavy metal ions from wastewater: a comprehensive and critical review, NPJ Clean Water 4 (1) (2021) 1–15, https://doi.org/10.1038/s41545-021-00127-0.
[17] S. Jadoun, J.P. Fuentes, B.F. Urbano, J. Yáñez, A review on adsorption of heavy metals from wastewater using conducting polymer-based materials, J. Environ. Chem. Eng. 11 (1) (2023) 1–13, https://doi.org/10.1016/j.jece.2022.109226.
[18] G. Crini, E. Lichtfouse, L.D. Wilson, N. Morin-Crini, Conventional and non-conventional adsorbents for wastewater treatment, Environ. Chem. Lett. 17 (1) (2019) 195–213, https://doi.org/10.1007/s10311-018-0786-8.
[19] A.M. Badran, U. Utra, N.S. Yussof, M.J.K. Bashir, Advancements in adsorption techniques for sustainable water purification: a focus on lead removal, Separations 10 (11) (2023) 1–26, https://doi.org/10.3390/separations10110565.
[20] B. Wang, J. Lan, C. Bo, B. Gong, J. Ou, Adsorption of heavy metal onto biomass-derived activated carbon: review, RSC Adv. 13 (7) (2023) 4275–4302, https://doi.org/10.1039/D2RA07911A.
[21] U. Upadhyay, I. Sreedhar, S.A. Singh, C.M. Patel, K.L. Anitha, Recent advances in heavy metal removal by chitosan based adsorbents, Carbohydr. Polym. 251 (2021) 1–29, https://doi.org/10.1016/j.carbpol.2020.117000.
[22] Anamika, V. Singh, B.K. Yadav, Adsorption study of heavy metals from aqueous solutions using magnetite nanoparticles, J. Phys. Conf. Ser. 1504 (1) (2020) 1–11, https://doi.org/10.1088/1742-6596/1504/1/012011.
[23] N.G. Kobylinska, V.G. Kessler, G.A. Seisenbaeva, O.A. Dudarko, In situ functionalized mesoporous silicas for sustainable remediation strategies in removal of inorganic pollutants from contaminated environmental water, ACS Omega 7 (27) (2022) 23576–23590, https://doi.org/10.1021/acsomega.2c02151.
[24] A.V. Samrot, M. Bavanilatha, S. Krithika Shree, M. Sathiyasree, J. Vanjinathan, N. Shobana, R. Thirugnanasambandam, C. Kumar, S. Wilson, D. Rajalakshmi, L.X. Noel Richard Prakash, R.S. Sanjay Preeth, Evaluation of heavy metal removal of nanoparticles based adsorbent using Danio rerio as model, Toxics 10 (12) (2022) 1–19, https://doi.org/10.3390/toxics10120742.
[25] E. Kuldeyev, M. Seitzhanova, S. Tanirbergenova, K. Tazhu, E. Doszhanov, Z. Mansurov, S. Azat, R. Nurlybaev, R. Berndtsson, Modifying natural zeolites to improve heavy metal adsorption, Water 15 (12) (2023) 1–11, https://doi.org/10.3390/w15122215.
[26] A. El-kordy, A. Elgamouz, E.M. Lemdek, N. Tijani, S.S. Alharthi, A.-N. Kawde, I. Shehadi, Preparation of sodalite and faujasite clay composite membranes and their utilization in the decontamination of dye effluents, Membranes 12 (1) (2021) 1–18, https://doi.org/10.3390/membranes12010012.
[27] N. Kordala, M. Wyszkowski, Zeolite properties, methods of synthesis, and selected applications, Molecules 29 (5) (2024) 1–25, https://doi.org/10.3390/molecules29051069.
[28] N. Sapawe, A.A. Jalil, S. Triwahyono, M.I.A. Shah, R. Jusoh, N.F.M. Salleh, B.H. Hameed, A.H. Karim, Cost-effective microwave rapid synthesis of zeolite NaA for removal of methylene blue, Chem. Eng. J. 229 (2013) 388–398, https://doi.org/10.1016/j.cej.2013.06.005.
[29] M. Hong, L. Yu, Y. Wang, J. Zhang, Z. Chen, L. Dong, Q. Zan, R. Li, Heavy metal adsorption with zeolites: the role of hierarchical pore architecture, Chem. Eng. J. 359 (2019) 363–372, https://doi.org/10.1016/j.cej.2018.11.087.
[30] E. Pérez-Botella, S. Valencia, F. Rey, Zeolites in adsorption processes: state of the art and future prospects, Chem. Rev. 122 (24) (2022) 17647–17695, https://doi.org/10.1021/acs.chemrev.2c00140.
[31] J. Přech, P. Pizarro, D.P. Serrano, J. Čejka, From 3D to 2D zeolite catalytic materials, Chem. Soc. Rev. 47 (22) (2018) 8263–8306, https://doi.org/10.1039/C8CS00370J.
[32] I.E. Bojaddayni, M.E. Küçük, Y.E. Ouardi, I. Jilal, S.E. Barkany, K. Moradi, E. Repo, K. Laatikainen, A. Ouammou, A review on synthesis of zeolites from natural clay resources and waste ash: recent approaches and progress, Miner. Eng. 198 (2023) 1–20, https://doi.org/10.1016/j.mineng.2023.108086.
[33] M. Król, Natural vs. synthetic zeolites, Crystals 10 (7) (2020) 1–8, https://doi.org/10.3390/cryst10070622.
[34] Y. Shi, X. Wang, C. Feng, W. Chen, S. Yang, Adsorption properties of natural zeolite supported by chitosan on Cd(II) in micropolluted irrigation water, ACS Omega 9 (1) (2024) 573–584, https://doi.org/10.1021/acsomega.3c06041.
[35] A. El-Kordy, A. Elgamouz, A. Abdelhamid, A.-N. Kawde, N. Tijani, E.M. Lemdek, Manufacturing of novel zeolite-clay composite membrane from natural clay and diatomite, an electrochemical study of the surface and application towards heavy metals removal, J. Environ. Chem. Eng. 12 (2) (2024) 1–14, https://doi.org/10.1016/j.jece.2024.112143.
[36] X. Huang, L. Lang, J. Li, C.S. Poon, Synthesis of Na-A zeolite loaded bentonite and its application for removal of Cu(II) from aqueous solutions, J. Water Process Eng. 56 (2023) 1–15, https://doi.org/10.1016/j.jwpe.2023.104359.
[37] D.K. Nguyen, V.P. Dinh, N.T. Dang, D.T. Khan, N.T. Hung, N.H. Thi Tran, Effects of aging and hydrothermal treatment on the crystallization of ZSM-5 zeolite synthesis from bentonite, RSC Adv 13 (30) (2023) 20565–20574, https://doi.org/10.1039/D3RA02552G.
[38] S.M. Seo, D. Kim, D. Kim, J.-H. Kim, Y.J. Lee, K.-M. Roh, I.-M. Kang, A simple synthesis of nitrate cancrinite from natural bentonite, J. Porous Mater. 25 (6) (2018) 1561–1565, https://doi.org/10.1007/s10934-018-0569-4.
[39] M. Esaifan, L.N. Warr, G. Grathoff, T. Meyer, M.T. Schafmeister, A. Kruth, H. Testrich, Synthesis of hydroxy-sodalite/cancrinite zeolites from calcite-bearing kaolin for the removal of heavy metal ions in aqueous media, Minerals 9 (8) (2019) 1–13, https://doi.org/10.3390/min9080484.
[40] H.S.Y. Akrawi, M.A. Al-Obaidi, C.H. Abdulrahman, Evaluation of Langmuir and Frendlich isotherm equation for Zinc Adsorption in some calcareous soil of Erbil province north of Iraq, IOP Conf. Ser. Earth Environ. Sci. 761 (2021) 1–10, https://doi.org/10.1088/1755-1315/761/1/012017.
[41] I. Langmuir, The adsorption ff gases on plane surfaces of glass, mica and platinum, J. Am. Chem. Soc. 40 (9) (1918) 1361–1403, https://doi.org/10.1021/ja02242a004.
[42] J. Wang, X. Guo, Adsorption isotherm models: classification, physical meaning, application and solving method, Chemosphere 258 (2020) 1–74, https://doi.org/10.1016/j.chemosphere.2020.127279.
[43] H.M.F. Freundlich, Over the adsorption in solution, J. Phys. Chem 57 (1906) 1100–1107.
[44] C.E. Almeida-Naranjo, M.B. Aldás, G. Cabrera, V.H. Guerrero, Caffeine removal from synthetic wastewater

using magnetic fruit peel composites: material characterization, isotherm and kinetic studies, Environ. Challenges. 5 (2021) 1–11, https://doi.org/10.1016/j.envc.2021.100343.
[45] R. Sips, On the structure of a catalyst Surface, J. Chem. Phys. 16 (1948) 490–495, https://doi.org/10.1063/1.1746922.
[46] S. Norouzi, M. Heidari, V. Alipour, O. Rahmanian, M. Fazlzadeh, F. Mohammadi-moghadam, H. Nourmoradi, B. Goudarzi, K. Dindarloo, Preparation, characterization and Cr(VI) adsorption evaluation of NaOH-activated carbon produced from Date Press Cake; an agro-industrial waste, Bioresour. Technol. 258 (2018) 48–56, https://doi.org/10.1016/j.biortech.2018.02.106.
[47] M.S.A. Zaher, S.M.A. Wahab, M. Taha, A.M. Masoud, Sorption characteristics of iron, fluoride and phosphate from wastewater of phosphate fertilizer plant using natural sodium bentonite, J. Membr. Sci. Technol. 8 (2) (2018) 1–10, https://doi.org/10.4172/2155-9589.1000186.
[48] J. Zhou, S. Zhang, H. Shi, J. Qiang, H. Dong, H. Liu, Hydrothermal synthesis of analcime from construction waste bricks and its adsorption mechanism for $Pb^{2+}$, Water, Air, Soil Pollut. 235 (186) (2024) https://doi.org/10.1007/s11270-024-06995-9.
[49] M.M.J. Treacy, J.B. Higgins, J.B. Higgins, Nepheline hydrate, in: Collect. Simulated XRD Powder Patterns Zeolites, Elsevier. 2001, pp. 192–193, https://doi.org/10.1016/B978-044450702-0/50094-0.
[50] L. Aloui, S. Mezghich, L. Mansour, S. Hraiech, F. Ayari, Swift removal of the heavy metals cadmium and lead from an aqueous solution by a CAN-zeolite synthesized from natural clay, ChemEngineering 7 (6) (2023) 1–17, https://doi.org/10.3390/chemengineering7060113.
[51] X. Ma, J. Yang, H. Ma, C. Liu, P. Zhang, Synthesis and characterization of analcime using quartz syenite powder by alkali-hydrothermal treatment, Microporous Mesoporous Mater. 201 (2015) 134–140, https://doi.org/10.1016/j.micromeso.2014.09.019.
[52] J.C. Buhl, Synthesis, hydrothermal stability and thermal reaction behavior of nepheline hydrate i (NHI), React. Kinet. Catal. Lett. 84 (2) (2005) 375–382, https://doi.org/10.1007/s11144-005-0232-3.
[53] J.C. Buhl, Synthesis and characterization of the basic and non-basic members of the cancrinite-natrodavyne family, Thermochim. Acta. 178 (1991) 19–31, https://doi.org/10.1016/0040-6031(91)80294-S.
[54] A.K. Mosai, H. Tutu, Recovery of platinum (IV) from aqueous solutions using 3-aminopropyl(diethoxy)methylsilane functionalized bentonite, J. Dispers. Sci. Technol. 43 (7) (2022) 1016–1027, https://doi.org/10.1080/01932691.2020.1847659.
[55] M.C. Barnes, J. Addai-Mensah, A.R. Gerson, A methodology for quantifying sodalite and cancrinite phase mixtures and the kinetics of the sodalite to cancrinite phase transformation, Microporous Mesoporous Mater. 31 (3) (1999) 303–319, https://doi.org/10.1016/S1387-1811(99)00080-3.
[56] G.D. Ventura, G.D. Gatta, G.J. Redhammer, F. Bellatreccia, A. Loose, G.C. Parodi, Single-crystal polarized FTIR spectroscopy and neutron diffraction refinement of cancrinite, Phys. Chem. Miner. 36 (4) (2009) 193–206, https://doi.org/10.1007/s00269-008-0269-8.
[57] S.M. Ibrahim, Z.T.A. Ali, Removal of acidic dye from aqueous solution using surfactant modified bentonite (organoclay): batch and kinetic study, J. Eng. 26 (5) (2020) 64–81, https://doi.org/10.31026/j.eng.2020.05.05.
[58] S. Salimkhani, K. Siahcheshm, A. Kadkhodaie, H. Salimkhani, Structural analysis and the effect of the chromium on LTA (Na) zeolite synthesized from kaolin, Mater. Chem. Phys. 271 (2021) 1–10, https://doi.org/10.1016/j.matchemphys.2021.124957.
[59] H. Wang, F. Zhang, R. Ang, D. Ren, Hydrothermal synthesis of cancrinite from coal gangue for the immobilization of Sr, Materials (Basel) 17 (3) (2024) 1–13, https://doi.org/10.3390/ma17030573.
[60] I.V. Joseph, A.M. Doyle, A. Amedlous, S. Mintova, L. Tosheva, Scalable solvent-free synthesis of aggregated nanosized single-phase cancrinite zeolite, Mater. Today Commun. 32 (2022) 1–6, https://doi.org/10.1016/j.mtcomm.2022.103879.
[61] A. Mannu, G. Vlachopoulou, V. Sireus, G. Mulas, G.L. Petretto, Characterization of Sardinian bentonite, J. Sci. Res. 11 (1) (2019) 145–150, https://doi.org/10.3329/jsr.v11i1.36900.
[62] K.A. Cychosz, M. Thommes, Progress in the physisorption characterization of nanoporous gas storage materials, Engineering 4 (4) (2018) 559–566, https://doi.org/10.1016/j.eng.2018.06.001.
[63] I. Alfikro, J. Jorena, E. Koriyanti, O.C. Satya, F. Monado, I. Royani, Evaluation of ferric ion adsorption on the surface imprinting adsorbent, Indones. J. Appl. Phys. 14 (2024) 353–364, https://doi.org/10.13057/ijap.v14i2.89893.
[64] Z. Bencheqroun, N.E. Sahin, O.S.G.P. Soares, M.F.R. Pereira, H. Zaitan, M. Nawdali, E. Rombi, A.M. Fonseca, P. Parpot, I.C. Neves, Fe(III)-exchanged zeolites as efficient electrocatalysts for Fenton-like oxidation of dyes in aqueous phase, J. Environ. Chem. Eng. 10 (3) (2022) 1–13, https://doi.org/10.1016/j.jece.2022.107891.
[65] S. Tahervand, M. Jalali, Sorption and desorption of potentially toxic metals (Cd, Cu, Ni and Zn) by soil amended with bentonite, calcite and zeolite as a function of pH, J. Geochemical Explor. 181 (2017) 148–159, https://doi.org/10.1016/j.gexplo.2017.07.005.
[66] Y. Lv, B. Ma, Y. Liu, C. Wang, Y. Chen, Adsorption behavior and mechanism of mixed heavy metal ions by zeolite adsorbent prepared from lithium leach residue, Microporous Mesoporous Mater. 329 (2022) 1–10, https://doi.org/10.1016/j.micromeso.2021.111553.
[67] L. Velarde, M.S. Nabavi, E. Escalera, M.-L. Antti, F. Akhtar, Adsorption of heavy metals on natural zeolites: a review, Chemosphere 328 (2023) 1–16, https://doi.org/10.1016/j.chemosphere.2023.138508.
[68] Iskandar Priyadi, R.R. Mukti Suwardi, Characteristics of heavy metals adsorption Cu, Pb and Cd using synthetics zeolite ZSM-5, J. Trop. Soils. 20 (2) (2016) 77–83, https://doi.org/10.5400/jts.2015.v20i2.77-83.
[69] M. Medykowska, M. Wiśniewska, K. Szewczuk-Karpisz, R. Panek, Interaction mechanism of heavy metal ions with the nanostructured zeolites surface – adsorption, electrokinetic and XPS studies, J. Mol. Liq. 357 (2022) 1–11, https://doi.org/10.1016/j.molliq.2022.119144.
[70] X. Long, R. Zhang, R. Rong, P. Wu, S. Chen, J. Ao, L. An, Y. Fu, H. Xie, Adsorption characteristics of heavy metals $Pb^{2+}$ and $Zn^{2+}$ by magnetic biochar obtained from modified AMD sludge, Toxics 11 (7) (2023) 1–16, https://doi.org/10.3390/toxics11070590.
[71] F. Pirvu, C.I. Covaliu-Mierlă, I. Paun, G. Paraschiv, V. Iancu, Treatment of wastewater containing nonsteroidal anti-inflammatory drugs using activated carbon material, Materials (Basel) 15 (2) (2022) 1–10, https://doi.org/10.3390/ma15020559.
[72] L.D. Castro-Alves, S. Yáñez-Vilar, M.A. González-Goméz, P. Garcia-Acevedo, Á. Arnosa-Prieto, Y. Piñeiro-Redondo, J. Rivas, Understanding adsorption mechanisms and metal ion selectivity of superparamagnetic beads with mesoporous CMK-3 carbon and commercial activated carbon, Microporous Mesoporous Mater. 374 (2024) 1–15, https://doi.org/10.1016/j.micromeso.2024.113159.
[73] D. Ghahremani, I. Mobasherpour, S.A. Mirhosseini, Sorption thermodynamic and kinetic studies of Lead removal from aqueous solutions by nano Tricalcium phosphate, Bull. La Société R. Des. Sci. Liège. 86 (2017) 96–112, https://doi.org/10.25518/0037-9565.7231.
[74] I. Senturk, H. Buyukgungor, F. Geyikci, Biosorption of phenol from aqueous solutions by the Aspergillus niger biomass: comparison of linear and non-linear regression analysis, Desalin. Water Treat. 57 (41) (2016) 19529–19539, https://doi.org/10.1080/19443994.2015.1102088.

[75] J. Serafin, B. Dziejarski, Application of isotherms models and error functions in activated carbon CO2 sorption processes, Microporous Mesoporous Mater. 354 (2023) 1–19, https://doi.org/10.1016/j.micromeso.2023.112513.
[76] V. Wernert, O. Schaef, L. Aloui, C. Chassigneux, F. Ayari, D. Ben Hassen Chehimi, R. Denoyel, Cancrinite synthesis from natural kaolinite by high pressure hydrothermal method: application to the removal of $Cd^{2+}$ and $Pb^{2+}$ from water, Microporous Mesoporous Mater. 301 (2020) 1–19, https://doi.org/10.1016/j.micromeso.2020.110209.
[77] Y. Kobayashi, F. Ogata, C. Saenjum, T. Nakamura, N. Kawasaki, Removal of $Pb^{2+}$ from aqueous solutions using K-type zeolite synthesized from coal fly ash, Water 12 (9) (2020) 1–12, https://doi.org/10.3390/w12092375.
[78] A.V. Borhade, T.A. Kshirsagar, A.G. Dholi, J.A. Agashe, Removal of heavy metals $Cd^{2+}$ , $Pb^{2+}$, and $Ni^{2+}$ from aqueous solutions using synthesized azide cancrinite, $Na_8[AlSiO_4]6(N_3)2.4(H_2O)$ 4.6, J. Chem. Eng. Data. 60 (3) (2015) 586–593, https://doi.org/10.1021/je500698x.
[79] N.S. Samanta, S. Banerjee, P. Mondal, Anweshan, U. Bora, M.K. Purkait, Preparation and characterization of zeolite from waste Linz-Donawitz (LD) process slag of steel industry for removal of $Fe^{3+}$ from drinking water, Adv. Powder Technol. 32 (9) (2021) 3372–3387, https://doi.org/10.1016/j.apt.2021.07.023.
[80] S. Bensafi, S. Amokrane, D. Nibou, Adsorption of $Cu^{2+}$, $Zn^{2+}$ and $Fe^{3+}$ ions in a ternary system from aqueous solutions on industrial waste 4A zeolite: characterization, dynamic, kinetic and thermodynamic studies, Colloid J. 87 (2025) 101–123, https://doi.org/10.1134/S1061933X24601148.
[81] F. Farid Ngatijo, D.S.P. Dika, Zeolite coating with phenantroline for adsorption of ion Fe (III), Adv. Eng. Res. 205 (2021) 31–35, https://doi.org/10.2991/aer.k.210825.007.
[82] T. Bakalár, M. Kaňuchová, A. Girová, H. Pavolová, R. Hromada, Z. Hajduová, Characterization of Fe(III) adsorption onto zeolite and bentonite, Int. J. Environ. Res. Public Health. 17 (16) (2020) 1–13, https://doi.org/10.3390/ijerph17165718.
[83] Z. Melichová, L. Hromada, Adsorption of $Pb^{2+}$ and $Cu^{2+}$ Ions from aqueous solutions on natural bentonite, Polish J. Environ. Stud. 22 (2012) 457–464.
[84] Y.S. Ho, G. McKay, Pseudo-second order model for sorption processes, Process Biochem. 34 (5) (1999) 451–465.
[85] L. Xia, Z. Huang, L. Zhong, F. Xie, C.Y. Tang, C.P. Tsui, Bagasse cellulose grafted with an amino-terminated hyperbranched polymer for the removal of Cr(VI) from aqueous solution, Polymers (Basel) 10 (8) (2018) 1–15, https://doi.org/10.3390/polym10080931.
[86] J. Kang, Y. Wang, Y. Qiu, The effect of $Fe^{3+}$ ions on the electrochemical behaviour of ocean manganese nodule reduction leaching in sulphuric acid solution, RSC Adv. 12 (2) (2022) 1121–1129, https://doi.org/10.1039/D1RA08440B.
[87] S. Kocaoba, Adsorption of Fe(II) and Fe(III) from aqueous solution by using sepiolite: speciation studies with MINEQL+ computer program, Sep. Sci. Technol. 55 (5) (2020) 896–906, https://doi.org/10.1080/01496395.2019.1579841.
[88] B. Chen, H. Guan, Y. Zhang, S. Liu, B. Zhao, C. Zhong, H. Zhang, W. Ding, A. Song, D. Zhu, L. Liu, B. Wulan, H. Li, G. Liu, X. Feng, Performance and mechanism of $Pb^{2+}$ and $Cd^{2+}$ ions' adsorption via modified antibiotic residue-based hydrochar, Heliyon 9 (4) (2023) e14930, https://doi.org/10.1016/j.heliyon.2023.e14930, 1-15.
[89] S. Xu, C. Zhou, X. Xu, K. Yang, Z. Wang, G. Liu, W. Wu, Synthesis of zeolite from biomass power plant ash for removal of $Pb^{2+}$ from solution: performance and mechanism, J. Environ. Chem. Eng. 13 (3) (2025) 1–13, https://doi.org/10.1016/j.jece.2025.116459.
[90] J. Mokrzycki, M. Fedyna, M. Marzec, J. Szerement, R. Panek, A. Klimek, T. Bajda, M. Mierzwa-Hersztek, Copper ion-exchanged zeolite X from fly ash as an efficient adsorbent of phosphate ions from aqueous solutions, J. Environ. Chem. Eng. 10 (6) (2022) 1–13, https://doi.org/10.1016/j.jece.2022.108567.
[91] F.S. Wanyonyi, F. Orata, G.K. Mutua, M.O. Odey, S. Zamisa, S.E. Ogbodo, F. Maingi, A. Pembere, Application of South African heulandite (HEU) zeolite for the adsorption and removal of $Pb^{2+}$ and $Cd^{2+}$ ions from aqueous water solution: experimental and computational study, Heliyon 10 (14) (2024) e34657, https://doi.org/10.1016/j.heliyon.2024.e34657, 1-14.
[92] X. Zhao, F. Gu, Y. Wang, Z. Peng, J. Liu, Surface electronegativity as an activity descriptor to screen oxygen evolution reaction catalysts of Li–O 2 battery, ACS Appl. Mater. Interfaces 12 (24) (2020) 27166–27175, https://doi.org/10.1021/acsami.0c04814.
[93] X. Fan, H. Liu, E. Anang, D. Ren, Effects of electronegativity and hydration energy on the selective adsorption of heavy metal ions by synthetic NaX zeolite, Materials (Basel) 14 (15) (2021) 1–16, https://doi.org/10.3390/ma14154066.
[94] W. Somyanonthanakun, R. Ahmed, V. Krongtong, S. Thongmee, Studies on the adsorption of Pb(II) from aqueous solutions using sugarcane bagasse-based modified activated carbon with nitric acid: kinetic, isotherm and desorption, Chem. Phys. Impact 6 (2023) 1–13, https://doi.org/10.1016/j.chphi.2023.100181.
[95] M.K. Sari, R. Basuki, B. Rusdiarso, Adsorption of Pb(II) from aqueous solutions onto humic acid modified by urea-formaldehyde: effect of pH, ionic strength, contact time, and initial concentration, Indones. J. Chem. 21 (6) (2021) 1371–1388, https://doi.org/10.22146/ijc.64600.
[96] L. Liu, S. Fan, Z. Wang, J. Hu, Chemical speciation distribution, desorption characteristics, and quantitative adsorption mechanisms of cadmium/lead ions adsorbed on biochars, Arab. J. Chem. 17 (4) (2024) 1–11, https://doi.org/10.1016/j.arabjc.2024.105669.
[97] S.P. Mishra, Adsorption–desorption of heavy metal ions, Curr. Sci. 107 (4) (2014) 601–612. http://www.jstor.org/stable/24103532.
[98] S. Indah, D. Helard, A. Binuwara, Studies on desorption and regeneration of natural pumice for iron removal from aqueous solution, Water Sci. Technol. 2017 (2) (2018) 509–515, https://doi.org/10.2166/wst.2018.177.
[99] N.A. Nguyen, D.K. Nguyen, V.P. Dinh, B.N. Duong, L. Ton-That, N.T. Hung, T.H. Ho, Effective adsorption of Pb(II) ion from aqueous solution onto ZSM-5 zeolite synthesized from Vietnamese bentonite clay, Environ. Monit. Assess. 195 (1530) (2023) 1–20, https://doi.org/10.1007/s10661-023-12153-1.
[100] A.E. Hidayat, S.S. Moersidik, S. Adityosulindro, Adsorption and desorption of zinc and copper in acid mine drainage onto synthesized zeolite from coal fly ash, J. Phys. Conf. Ser. 1811 (1) (2021) 1–8, https://doi.org/10.1088/1742-6596/1811/1/012045.
[101] W. Rudzinski, W. Plazinski, Kinetics of metal ions adsorption at heterogeneous solid/solution interfaces: a theoretical treatment based on statistical rate theory, J. Colloid Interface Sci. 327 (1) (2008) 36–43, https://doi.org/10.1016/j.jcis.2008.07.048.
[102] K. Mitsumoto, K. Takae, Elastic heterogeneity governs asymmetric adsorption–desorption in a soft porous crystal, Proc. Natl. Acad. Sci. 120 (30) (2023) 1–9, https://doi.org/10.1073/pnas.2302561120.
[103] M. Senila, O. Cadar, Modification of natural zeolites and their applications for heavy metal removal from polluted environments: challenges, recent advances, and perspectives, Heliyon 10 (3) (2024) e25303, https://doi.org/10.1016/j.heliyon.2024.e25303, 1-17.
[104] S. Buzukashvili, R. Sommerville, O. Kökkõlõç, P. Ouzilleau, N.A. Rowson, K.E. Waters, Exploring efficiency and regeneration of magnetic zeolite synthesized from coal fly ash for water treatment applications, JCIS Open 17 (2025) 1–12, https://doi.org/10.1016/j.jciso.2024.100127.